Initial Operation of the Scintillator-Based Fast-Ion Loss Detector Rotary and Reciprocating System in MAST-U

J. F. Rivero-Rodriguez, L. Velarde, T. Williams, J. Galdón-Quiroga, M. García-Muñoz, K. G. McClements, the EUROfusion Tokamak Exploitation Team, and the MAST-U Team

***Abstract*— The first scintillator-based fast-ion loss detector (FILD) was installed in MAST-U as part of its main upgrade and it was commissioned during the first experimental campaign. FILD works as a magnetic spectrometer, directly measuring neutral beam injector (NBI) fast-ion losses using a scintillator plate that emits light when fast ions impinge on it. Yttrium aluminum garnet activated by cerium (YAG:Ce) is used as the scintillator material in MAST-U, which has a decay time in the range of 100 ns. This, in combination with an avalanche photodiode (APD) camera at sampling rates up to 4 MHz, has made it possible to detect fast-ion loss fluctuations at frequencies up to 2 MHz, an unprecedented measurement for any scintillator-based FILD. The probe is protected from the plasma loads with a cap made of 15-μm grain graphite, similar to the divertor tiles. The probe is installed on an in-vessel rotary and reciprocating system actuated with bellow-based feed-throughs and a pair of stepper motors that make it possible to operate remotely on a shot-to-shot basis. The rotary actuator adapts the probe orientation to the magnetic field pitch and the reciprocating actuator adapts the probe radial distance to the separatrix. An infrared camera monitoring the temperature on the graphite cap showed that the temperature increase during a shot is lower than 20 °C. The impurities added to the plasma by the FILD probe have been monitored using spectroscopy measurements. The operation of the MAST-U FILD provides a source of lessons learned for the design of future reciprocating diagnostics such as the ITER FILD.**

***Index Terms*— Diagnostics, energetic particles, fusion energy, spherical tokamaks.**

I. Introduction

FAST ions, that is, ions whose energy is well above the typical temperature of the bulk ions, play a crucial role in magnetically confined fusion as they provide the heating and current drive to achieve burning plasmas [1]. Keeping good fast-ion confinement is necessary to enable energy transfer from the fast ions to the bulk plasma. In addition, as they are highly energetic particles, fast-ion losses may endanger plasma-facing components of the tokamak wall [2]. Therefore, understanding the fast-ion transport and predicting the losses is key to achieving high fusion performance and safe tokamak operation. Fast-ion losses may be enhanced by a wide range of mechanisms, such as charge exchange, Coulomb collisions, or interactions with magnetohydrodynamic (MHD) instabilities, making this topic an important field of research in fusion energy.

The Mega-Amp Spherical Tokamak Upgrade (MAST-U) [3] is one of the largest low-aspect-ratio tokamaks worldwide, together with NSTX-U [4]. One of the main objectives of MAST-U is to study fast-ion physics that is relevant for spherical tokamaks and future burning plasmas. MAST-U is equipped with two neutral beam injectors (NBIs) that provide up to 5 mW of external heating and inject particles at energies up to 75 keV. Since fusion product ions are not confined in MAST-U, the NBIs are the only source of confined fast ions. However, spherical tokamaks like MAST-U operate at relatively low magnetic fields compared to conventional tokamaks. Thus, the NBI fast-ion speed in MAST-U is above the Alfvén speed of the plasma. Such a super-Alfvénic fast-ion population mimics some of the conditions of fusion-born ions in burning plasmas, thus making it possible to study fast-ion dynamics that are relevant for future fusion devices like ITER. MAST-U is equipped with several fast-ion diagnostics that make it possible to study the confined fast-ions with the comprehensive spatial and temporal resolution, including a fast-ion deuterium-α (FIDA) spectrometer [5], that measures Doppler-shifted Balmer-α emission due to charge exchange between fast ions and neutrals; a solid-state neutral particle analyzer (SSNPA) [6] that detects fast neutrals from charge exchange reactions; a neutron camera upgrade (NCU) [7], that measures the neutron flux along six lines of sight on the equatorial plane; and a proton detector (PD) [8], that measures unconfined fusion protons. Since highly energetic neutrons and protons mainly result from beam–target fusion reactions, they provide indirect measurements of fast ions in the plasma.

During the major upgrade of MAST-U, a scintillator-based fast-ion loss detector (FILD) was designed and built [9]. FILD provides direct measurements of fast ions losses with

Manuscript received 3 October 2023; revised 8 March 2024; accepted 3 May 2024. This work has been carried out within the framework of the EUROfusion Consortium, funded by the European Union via the Euratom Research and Training Programme (Grant Agreement No 101052200 — EUROfusion) and from the Engineering and Physical Sciences Research Council (EPSRC) [grant number EP/W006839/1]. The work of J. Galdón-Quiroga was supported by the Marie Skłodowska-Curie Actions (MSCA) Postdoctoral Fellowship (FP) Program under Grant 101069021. The review of this article was arranged by Senior Editor R. Chapman. *(Corresponding author: J. F. Rivero-Rodriguez.)*

J. F. Rivero-Rodriguez and K. G. McClements are with Culham Science Centre, United Kingdom Atomic Energy Authority, OX14 3DB Abingdon, U.K. (e-mail: juan.rivero-rodriguez@ukaea.uk).

L. Velarde is with the Departamento de Ingeniería Energética, Universidad de Sevilla, 41004 Seville, Spain.

T. Williams is with the Department of Physics and Astronomy, University of Exeter, EX4 4PY Exeter, U.K.

J. Galdón-Quiroga and M. García-Muñoz are with the Departamento de Física Atómica, Molecular y Nuclear, Universidad de Sevilla, 41004 Seville, Spain.

Color versions of one or more figures in this article are available at https://doi.org/10.1109/TPS.2024.3400017.

Digital Object Identifier 10.1109/TPS.2024.3400017

velocity–space resolution to resolve the fast-ions pitch angle ($\Lambda = \arccos(v_\parallel/v)$) and gyroradius ($\rho_L = (mv_\perp/qB)$), and temporal resolution to resolve their loss frequency. The scintillator-based FILD is the reference diagnostic to detect fast-ion losses in most large tokamaks, including TFTR [10], JET [11], [12], and NSTX [13]. In fact, a scintillator-based FILD for ITER is currently under design [14], [15], [16]. FILD is considered a suitable diagnostic to measure fusion-born α-particles in future devices, where the aforementioned techniques may work only marginally due to the low interaction between 3.5 MeV α-particles and the bulk plasma. The MAST-U FILD will be an extensive source of lessons learned for future devices like ITER. The MAST-U FILD is optimized to measure NBI fast-ions in a wide velocity–space range and at frequencies up to around $f_{ci}/2$, where f_{ci} is the ion cyclotron frequency. The probe is mounted on a rotary and reciprocating mechanism to adapt the probe orientation and radial position to the magnetic field pitch and plasma shape corresponding to a wide range of scenarios. The diagnostic was brought into operation in 2021, and its systems have been gradually commissioned ever since. This article reports on the installation, commissioning, and operation of the MAST-U FILD data acquisition system, and its rotary and reciprocating mechanism.

The article is structured as follows. Section II introduces the MAST-U FILD data acquisition system. Section III presents the in-vessel rotary and reciprocating mechanism and the external actuators that remotely control it. Section IV discusses the first operation of the reciprocating system. Section V looks into the main lessons learned from the commissioning and first operation of the MAST-U FILD. Finally, Section VI provides a summary of the diagnostic status and an outlook.

II. Data Acquisition System

FILD works as a magnetic spectrometer, as shown in Fig. 1. It consists of a small slit that collimates the fast ions and disperses them onto a scintillator plate, which emits light from the fast-ion strike points. Influenced by the Tokamak magnetic field, the fast-ions follow helical orbits that, depending on their pitch angle and gyroradius, will hit the scintillator plate at different locations. This makes it possible to infer the fast-ion velocity space from the location of the light emitted by the scintillator plate [17]. Therefore, the resolution and range of the measurements strongly depend on the slit geometry and the relative positions of the slit and the scintillator plate. The designed geometry, described in [9], provides measurements in the range of $\rho_L = [3.5, 21\ \text{cm}]$ and $\Lambda = [30°, 85°]$. This offers enough range to measure fast ions above approximately 4 keV. In particular, the slit geometry is optimized to measure 75-keV NBI ions in a target plasma current of 2 MA, whose gyroradii are $\rho_L \sim 10$ cm. Nonetheless, FILD also provides enough range for the existing scenarios with plasma currents from 450 kA ($\rho_L \sim 17$ cm) to 750 kA ($\rho_L \sim 15$ cm), with an approximate magnetic field at the magnetic axis of 0.56 and 0.61 T, respectively. To collect the fast ions escaping from the plasma, the slit must be close enough to the last closed flux surface (LCFS). Therefore, the main components of the FILD probe are protected against the heat loads from the bulk

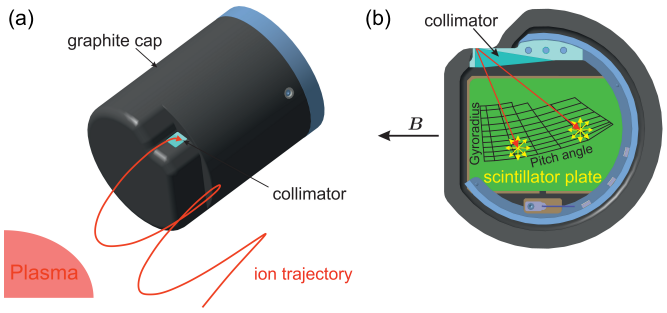

Fig. 1. (a) FILD probe head and escaping fast-ion orbit reaching the collimator slit. (b) Scintillator plate where the collimated ions are dispersed using the tokamak magnetic field and characterized by their gyroradius and pitch angle. Reproduced with permission from [9].

plasma and the impinging fast ions by a protective cap made of the same fine-grain graphite as the divertor tiles. This material provides a reasonably low thermal conductivity of 90 W/(mK) while not adding unexpected elements to the vacuum vessel.

The properties of the scintillator material and the data acquisition system directly affect the quality and the temporal and spatial resolution of the recorded data. The scintillator material is yttrium aluminum garnet activated by cerium (YAG:Ce) in the form of powder deposited on a 2 mm stainless steel plate. YAG:Ce, also dubbed P46, has a decay time of 70 ns, making it possible in principle to detect fast-ion loss fluctuations with frequencies up to 10 MHz. On the other hand, it has a relatively low photon yield [18] that is nonetheless sufficient to cover the dynamic range of the data acquisition system. The data acquisition system consists of two cameras with direct sight to the scintillator plate through a window port. The cameras record the light emitted simultaneously using a 50/50 beam splitter to combine measurements of the gradually evolving phase space and the fast fluctuations of the losses. The former is a complementary metal oxide semiconductor (CMOS) camera with 1-Mpx resolution, 3.5-kHz maximum sampling rate, and a maximum signal-to-noise ratio of 41 dB. This camera provides sufficient spatial resolution to infer the velocity space of the losses and enough temporal resolution to detect the losses induced by bursting plasma instabilities. The high time resolution camera is an APDCAM-10G [19], that consists of an 8×8 array of avalanche photodiodes (APDs), distributed in a rectangular sensor. The APDCAM-10G provides data from each APD with a sampling rate of 4 MHz, a maximum amplitude of 1.8 V, and a root mean square (rms) noise of 5 mV. The APDCAM-10G enables Fourier analysis of the losses, making it possible to infer the frequency of the losses coherent with MHD instabilities with frequencies up to 2 MHz. Moreover, the APDCAM-10G includes 4 LEDs around its sensor, whose light can be observed on the scintillator plate, when the camera is properly aligned and focused. This makes it possible to align the CMOS camera with respect to the APDCAM-10G, and hence to detect the velocity space fluctuations in the losses at frequencies higher than the Nyquist frequency of the CMOS camera, as the velocity–space data is complemented with the high sampling rate data from the APDCAM-10G.

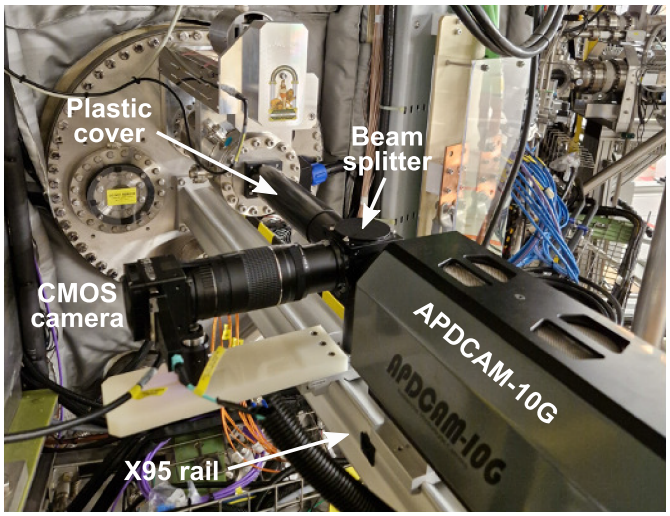

Fig. 2. Assembly of the FILD data acquisition system.

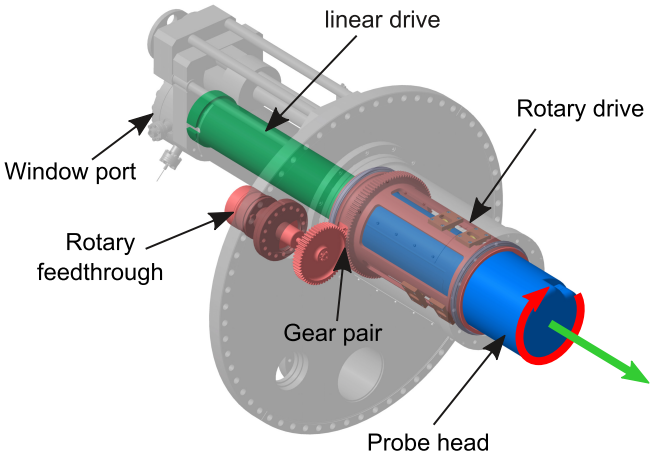

Fig. 3. Diagram of the rotary (red) and reciprocating (green) mechanism that drives the MAST-U FILD probe head (blue). Reproduced with permission from [9].

While the scintillator plate is an in-vessel component installed in the FILD probe, the cameras and lenses are mounted on an X95 rail outside the vessel, as shown in Fig. 2. This offers easy accessibility to align and calibrate the diagnostic. To achieve a light-tight data acquisition system, the optical system is covered by a plastic tube bolted to the window port. In turn, the plastic cover acts as a connector between the moving parts of the diagnostic and the optical system fixed to the X95 rail. As the reciprocating mechanism moves the window port, the plastic cover slides over the optical system keeping a light-tight field of view between the scintillator plate and the optical system. Unlike the cameras in other fusion devices, the MAST-U FILD cameras are not shielded from radiation or magnetic fields as the expected neutron rate (10^{14} s^{-1}) and magnetic field (0.05 T) are within the operational limits of the cameras.

III. Rotary and Reciprocating Mechanism

The FILD signal directly depends on the fast ions gyroradii, the tokamak magnetic field, and the probe's distance to the LCFS. The scintillator plate needs to be sufficiently large to cover gyroradii $\leq$21 cm in MAST-U. This led to a probe head with an outer diameter of 15 cm, which determined the size of the supporting structure. As the plasma current and the toroidal magnetic field are parameters commonly used to perform experimental scans, which modify the magnetic field pitch, a good magnetic field alignment with the collimator slit is necessary to maximize the range in pitch angle. The magnetic field pitch relative to the horizontal plane at the FILD probe ranges from around 23° in 450 kA plasmas to 52° in future 2 MA scenarios. This motivated the design of a rotary mechanism that adapts the slit orientation to the tokamak magnetic field within the range [0°, 90°], combined with a reciprocating mechanism that adapts its distance to the plasma, R = [1.45, 1.60 m]. The FILD probe is mounted on a telescopic system that enables the simultaneous radial movement and rotation of the probe head, as shown in Fig. 3. The probe is sitting on a rotary drive that transfers its rotation to the probe head. In turn, the rotation is transferred from an out-vessel rotary feedthrough to the rotary drive with a self-locking gear pair. The probe head is pushed and pulled by a linear drive that is connected to a bellow-based linear feedthrough. The light emitted by the scintillator plate travels inside the light-tight telescopic mechanism, up to a window port at the rear of the in-vessel system, where it is captured by the data acquisition system described in Section II.

The mechanical system is installed inside the vacuum vessel. Thus, the structural components are made of nonmagnetic vacuum-compatible stainless steel, and the ball bearings consist of silicon nitride balls with low friction rails and no lubrication. Additionally, the gear pair uses brass gear and stainless steel gear to avoid cold welding between their contact points. The tolerances between the graphite cap and the stainless steel mechanism have been designed to allow for a 200 °C thermal expansion during the baking of the vacuum vessel. This is found to be the most critical stage of the system, as the mechanism is otherwise at room temperature of approximately 25 °C. The mechanism stays at moderate temperatures even during plasma operations, when the heat load is mostly sustained by the graphite cap. The diagnostic has undergone two bakes of the vacuum vessel without damage.

As shown in Fig. 4, the linear feedthrough consists of a metallic bellow that is compressed and expanded by a worm gear. This pushes and pulls the in-vessel linear drive that transfers the movement to the probe head. The worm gear is actioned by a stepper motor, enabling remote control of the FILD position between shots at low speed (<10 cm/min) and high precision (<1 mm/step). The stepper motor is shielded with a stainless steel Faraday cage to avoid interference with the tokamak magnetic field. The rotary feedthrough consists of a bent shaft covered by a metallic bellow. The bent shaft is rotated from outside the vessel to transfer the rotation to the in-vessel gear pair. A stepper motor was added to the rotary feedthrough to enable the remote control of the probe orientation. However, due to the internal friction of the in-vessel mechanism, the stepper motor's maximum torque (2 Nm) was not sufficient to rotate the probe. Therefore, the

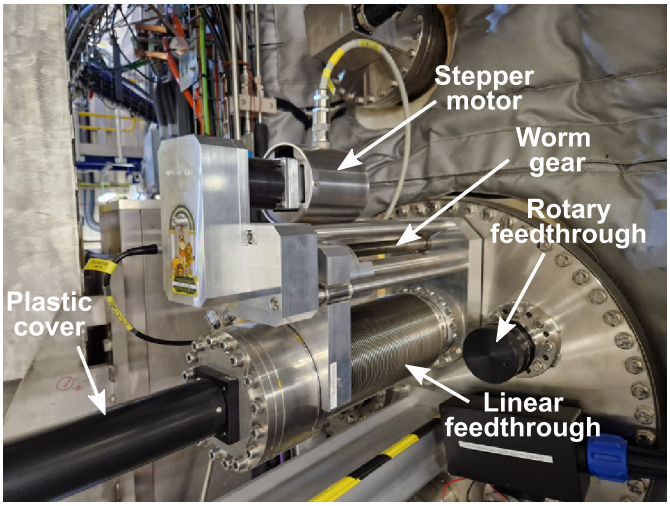

Fig. 4. Out-vessel feed-throughs of the FILD rotary and reciprocating mechanism.

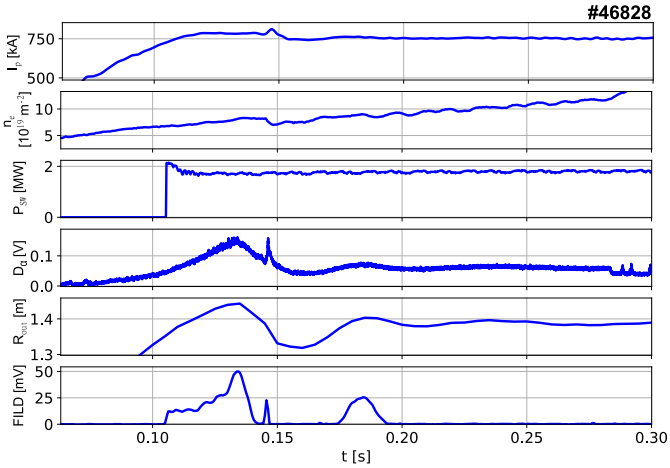

Fig. 5. From top to bottom, plasma current, line integrated electron density, off-axis NBI power, D_α emission, plasma outer radius, and FILD signal of MAST-U plasma shot #46828.

stepper motor was replaced by a manual knob that enables a maximum torque of 5 Nm. This was enough to overcome the internal friction of the mechanism and rotate the probe head. As a consequence, the probe's rotation is possible only on nonoperational days, when access to the diagnostic is permitted. The feed-throughs are equipped with encoders and limit switches that record the radial and rotational coordinates of the diagnostic on a shot-to-shot basis.

IV. Operation of the FILD Reciprocating Probe

The first operation of the FILD reciprocating probe was carried out with the setup described in Sections II and III. This is, the fast-ion losses were recorded simultaneously with the CMOS and the APDCAM-10G cameras, the orientation of the probe was fixed during operational days, and the reciprocating system was controlled remotely. Additionally, the temperature of the graphite cap was monitored with an infrared camera, as it is proven to be a good method of monitoring the FILD overheating [20]. The FILD probe includes a thermocouple to monitor its temperature but it has not been commissioned yet. The MAST-U plasma shot employed to optimize the FILD position was #46828, a 750-kA plasma with a conventional double-null divertor configuration, 0.61 T at the magnetic axis and a nominal outer major radius of 1.39 m, heated with off-axis NBI providing a total power of 1.8 mW. The plasma outer radius was controlled with a real-time feedback control. The FILD radial position, defined as the distance from the innermost face of the probe head to the center of the tokamak column, was $R = 1.52$ m. Thus, the nominal distance to the plasma LCFS was 0.13 m. However, the outer radius feedback control showed an unintentional underdamped (oscillatory) phase at the beginning of the shot, as can be observed in Fig. 5, meaning that the plasma reached a major radius close to 1.44 m during the overshoot, reducing the FILD relative distance to the plasma to 0.08 m. This resulted in a clear increase of the FILD signal during the unintentional overshoot, indicating a correlation between the FILD signal and its relative distance to the LCFS. This correlation is

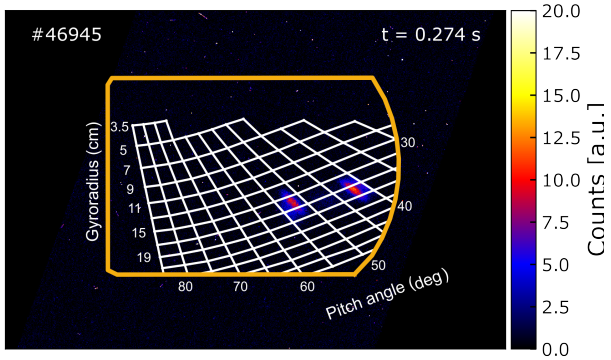

Fig. 6. Frame of the CMOS camera in MAST-U shot #46945 at $t = 0.274$ s. The scintillator plate contour is shown in yellow and the velocity–space strike map is shown in white.

evident in all channels of the APDCAM-10G, showing an increase in total losses. Although this behavior is expected, as a reduced distance to the LCFS means that the probe is closer to marginally confined fast-ion orbits that can be detected, it shows that the probe is not shaded by other plasma-facing components. The results are employed in shot #46945, using the same plasma parameters as in #46828, heated by two beams and with a nominal outer radius of 1.41 m. The probe radial distance was 1.50 m, resulting in a relative distance of 0.09 m. This made it possible to measure the velocity–space of the losses with the CMOS camera during the flat-top phase of the discharge, as shown in Fig. 6. The frame shows two separate spots, corresponding to the prompt-loss velocity–space of each beam.

Fig. 5 also shows an increase in D_α emission correlated with the outer radius behavior. A fast camera recording the plasma emission in the visible spectrum revealed a glow in the proximity of the FILD probe correlated with this increase in D_α emission. The glow could be an indication of the probe overheating or a release of impurities from the FILD probe to the plasma, which could present a concern for the operation of the diagnostic and MAST-U. However, the postshot temperature (<1 s after the shot ended) of the FILD probe was 36.3 °C, showing an increase of 5 °C with respect

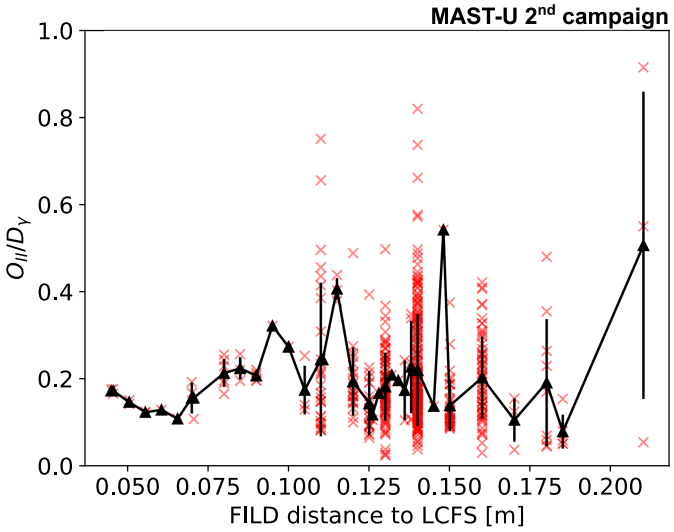

Fig. 7. O_{II}/D_γ emission ratio versus FILD relative distance to the LCFS for a dataset of plasma shots from the second MAST-U experimental campaign in red. The mean and standard deviation of the emission ratios for each relative distance are shown in black.

to the preshot measurement. This excludes the possibility of the probe glowing due to a drastic overheating. Moreover, a comprehensive analysis of spectrometry data from a dataset of plasma shots from the second MAST-U experimental campaign showed that the ratio of O_{II}/D_γ emission (considered an estimate of the oxygen released from the wall into the scrape-off layer) did not correlate with the insertion of FILD, as can be observed in Fig. 7. A similar result was obtained comparing the C_{II} emission against D_γ emission, indicating that the FILD insertion does not affect the impurities present in the plasma. The glow observed in the visible spectrum when the plasma is close to the FILD probe is probably due to a Debye sheath forming around the graphite cap. The Debye length in MAST-U, which establishes the width of the Debye sheath, is $\lambda_D = ((\varepsilon_0 T_e)/(e^2 n_e))^{1/2} \approx 24\ \mu$m, where ε_0 is the vacuum permittivity, $T_e = 100$ eV is the edge electron temperature ($R = 1.4$ m), e is the electron charge and $n_e = 10^{19}$ m^{-3} is the edge electron density ($R = 1.4$ m). The Debye sheath itself might not be large enough to explain the observations. However, the Debye sheath is commonly preceded by a presheath dominated by collision and ionization processes, whose width could be up to a thermal ion gyroradius ($\sim$1.5 cm) in strongly magnetized conditions [21]. Such an ionization region explains the observations in the visible spectrum. It should be noted that other plasma-facing components produce a similar emission in the visible camera during the outer radius overshoot, and the increase in D_α emission is also observed in plasma shots when the outer radius oscillates even if FILD is not inserted. Thus, the outer radius overshoot was reduced in subsequent shots, making it possible to insert the FILD down to $R = 1.455$ m with no indications of overheating, and a signal-to-noise ratio $>$100.

V. Lessons Learned

The installation and commissioning of the MAST-U FILD has brought a collection of lessons learned that are relevant for the installation of many fusion diagnostics. The FILD cameras were installed and commissioned in a gradual process. First, a CCD camera with a sampling rate of 23 Hz was installed at the beginning of the first MAST-U campaign. Although this gave limited information on the fast-ion losses, it made it possible to commission other FILD subsystems, such as the scintillator response and the probe orientation. Then, the APDCAM-10G was installed, detecting fast-ion loss fluctuations at frequencies up to 2 MHz with limited information on their velocity space. In the second MAST-U campaign, the beam splitter and the CMOS camera were installed, completing the data acquisition system described in Section II. This showed the benefits of an agile approach of continuous improvement, in which a minimum viable product was identified in each experimental campaign. It provided useful experimental data from the early stages of the diagnostic commissioning and it allowed the operators to anticipate possible obstacles in the installation of the final data acquisition system. On the other hand, a flexible and accessible optical system and the elaboration of repeatable procedures to align and calibrate the FILD cameras provide good camera alignment that enables simultaneous determination of the velocity space and the frequency of the fast-ion losses.

Initially, the APDCAM-10G data showed 6-kHz interference, matching the switching frequency of the main power supplies in MAST-U. To mitigate this interference, several modifications were made. The APDCAM-10G was isolated from the vacuum vessel and covered with a Faraday cage to avoid any electrostatic interference from the environment, although these had little effect on the data. Also, the electric diagram of the data acquisition system was reviewed and the APDCAM-10G power supplies were modified so that they were earthed from the diagnostic cubicle, as they were found to be electrically floating. With this, the interference was reduced by an order of magnitude, achieving a rms noise level of 5 mV. This shows the importance of a good electrical diagram and a clean machine earth to avoid interference in diagnostic data. After this, the main source of noise is due to neutron radiation, although it affects individual pixels at a rate of 100 s^{-1}, so it is easily removed from the data. Nevertheless, this highlights the importance of shielding data acquisition systems from radiation in future devices.

The in-vessel mechanism is installed in a vacuum environment where the use of lubricants is not permitted. Although the internal friction of the mechanism was minimized, it was sufficient to limit the operation of the external actuator. A stepper motor with a maximum torque of 5 Nm will be installed in the next campaign to enable remote control of the FILD orientation. Nevertheless, this illustrates the point that the effect of internal friction must be addressed in future diagnostics, such as the ITER FILD. This will require the prototyping of their mechanisms to estimate their internal friction.

The first operation of the MAST-U FILD has demonstrated the reliable performance of the reciprocating system, an infrared camera being used to monitor the probe temperature. The FILD signal shows a clear correlation with the probe's relative distance to the plasma. This has been exploited in further experiments to optimize the FILD position, minimizing the number of shots required. On the other hand, good control of the plasma outer radius is key to providing stable measurements of the fast-ion losses.

VI. Summary

The first scintillator-based FILD in MAST-U is equipped with a fast scintillator material and a data acquisition system that combines a high spatial resolution camera with a high temporal resolution camera, providing information on the velocity space and frequency of the losses, respectively. A rotary and reciprocating mechanism offers excellent adaptability to different magnetic field pitches and plasma major radii. The material selection and tolerances of the in-vessel components avoid cold welding and allow for 200°C baking for the diagnostic conditioning. Remote control of the reciprocating system was successfully commissioned, making it possible to modify the FILD radial position on a shot-to-shot basis.

The MAST-U FILD has been fully operational since the second MAST-U experimental campaign. The first operation of the reciprocating system revealed a correlation between the amplitude of the FILD signal and the distance between the probe and the LCFS. This has expanded the working window of the MAST-U FILD and enabled measurements of the fast-ion velocity space during the flat-top phase of the discharge. Moreover, ongoing experiments are combining the infrared cameras and FILD to assess the fast-ion losses in MAST-U using infrared thermography. This article shows that the operation of a reciprocating diagnostic in MAST-U is safe for both the diagnostic and the plasma operation, and it outlines the necessary monitoring and control systems to achieve this. Thus, the MAST-U FILD has become a source of lessons learned for future reciprocating diagnostics such as the ITER FILD. The diagnostic supports dedicated studies on fast-ion losses induced by plasma instabilities in spherical tokamaks and on the effect of externally applied magnetic perturbations on fast-ion confinement [22], [23], [24].

Acknowledgment

To obtain further information on the data and models underlying this article please contact PublicationsManager@ukaea.uk. Views and opinions expressed are however those of the authors only and do not necessarily reflect those of the European Union or the European Commission. Neither the European Union nor the European Commission can be held responsible for them.

The members of the EUROfusion Tokamak Exploitation Team are D. Abate, J. Adamek, M. Agostini, C. Albert, F. C. P. Albert Devasagayam, S. Aleiferis, E. Alessi, J. Alhage, S. Allan, J. Allcock, M. Alonzo, G. Anastasiou, E. AnderssonSunden, C. Angioni, Y. Anquetin, L. Appel, G. M. Apruzzese, M. Ariola, C. Arnas, J. F. Artaud, W. Arter, O. Asztalos, L. Aucone, MH. Aumeunier, F. Auriemma, J. Ayllon, E. Aymerich, A. Baciero, F. Bagnato, L. Bähner, F. Bairaktaris, P. Balázs, L. Balbinot, I. Balboa, M. Balden, A. Balestri, M. Baquero Ruiz, T. Barberis, C. Barcellona, O. Bardsley, M. Baruzzo, S. Benkadda, T. Bensadon, E. Bernard, M. Bernert, H. Betar, R. Bianchetti Morales, J. Bielecki, R. Bilato, P. Bilkova, W. Bin, G. Birkenmeier, R. Bisson, P. Blanchard, A. Bleasdale, V. Bobkov, A. Boboc, A. Bock, K. Bogar, P. Bohm, T. Bolzonella, F. Bombarda, N. Bonanomi, L. Boncagni, D. Bonfiglio, R. Bonifetto, M. Bonotto, D. Borodin, I. Borodkina, t.o.s.j.bosman, C. Bourdelle, C. Bowman, S. Brezinsek, D. Brida, F. Brochard, R. Brunet, D. Brunetti, V. Bruno, R. Buchholz, J. Buermans, H. Bufferand, P. Buratti, A. Burckhart, J. Cai, R. Calado, J. Caloud, S. Cancelli, F. Cani, B. Cannas, M. Cappelli, S. Carcangiu, A. Cardinali, S. Carli, D. Carnevale, M. Carole, M. Carpita, D. Carralero, F. Caruggi, I. S. Carvalho, I. Casiraghi, A. Casolari, F.J. Casson, C. Castaldo, A. Cathey, F. Causa, J. Cavalier, M. Cavedon, J. Cazabonne, M. Cecconello, L. Ceelen, A.Celora, J. Cerovsky, C.D. Challis, R. Chandra, A. Chankin, B. Chapman, H. Chen, M. Chernyshova, A. G. Chiariello, P. Chmielewski, A. Chomiczewska, C. Cianfarani, G. Ciraolo, J. Citrin, F. Clairet, S. Coda, R. Coelho, J. W. Coenen, I.H. Coffey, C. Colandrea, L. Colas, S. Conroy, C. Contre, NJ. Conway, L. Cordaro, Y. Corre, D. Costa, S. Costea, D. Coster, X. Courtois, C. Cowley, T. Craciunescu, G. Croci, A. M. Croitoru, K. Crombe, D. J. Cruz Zabala, G. Cseh, T. Czarski, A. Da Ros, A. Dal Molin, M. Dalla Rosa, Y. Damizia, O. D'Arcangelo, P. David, M. De Angeli, E. De la Cal, E. De La Luna, G. De Tommasi, J. Decker, R. Dejarnac, D. Del Sarto, G. Derks, C. Desgranges, P. Devynck, S. Di Genova, L. E. di Grazia, A. Di Siena, M. Dicorato, M. Diez, M. Dimitrova, T. Dittmar, L. Dittrich, J. J. DomínguezPalacios Durán, P. Donnel, D. Douai, S. Dowson, S. Doyle, M. Dreval, P. Drews, L. Dubus, R. Dumont, D. Dunai, M. Dunne, A. Durif, F. Durodie, G. DurrLegoupilNicoud, B. Duval, R. Dux, T. Eich, A. Ekedahl, S. Elmore, G. Ericsson, J. Eriksson, B. Eriksson, F. Eriksson, S. Ertmer, A. Escarguel, B. Esposito, T. Estrada, E. Fable, M. Faitsch, N. Fakhrayi Mofrad, A. Fanni, T. Farley, M. Farník, N. Fedorczak, F. Felici, X. Feng, J. Ferreira, D. Ferreira, N. Ferron, O. Fevrier, O. Ficker, A.R. Field, A. Figueiredo, N. Fil, D. Fiorucci, M. Firdaouss, R. Fischer, M. Fitzgerald, M. Flebbe, M. Fontana, J. Fontdecaba Climent, A. Frank, E. Fransson, L. Frassinetti, D. Frigione, S. Futatani, R. Futtersack, S. Gabriellini, D. Gadariya, D. Galassi, K. Galazka, J. Galdon, S. Galeani, D. Gallart, A. Gallo, C. Galperti, M. Gambrioli, S. Garavaglia, J. Garcia, M. Garcia Munoz, J. Gardarein, L. Garzotti, J. Gaspar, R. Gatto, P. Gaudio, M. Gelfusa, J. Gerardin, S.N. Gerasimov, R. Gerru Miguelanez, G. Gervasini, Z. Ghani, F. M. Ghezzi, G. Ghillardi, L. Giannone, S. Gibson, L. Gil, A. Gillgren, E. Giovannozzi, C. Giroud, G. Giruzzi, T. Gleiter, M. Gobbin, V. Goloborodko, A. González Ganzábal, T. Goodman, V. Gopakumar, G. Gorini, T. Görler, S. Gorno, G. Granucci, D. Greenhouse, G. Grenfell, M. Griener, W. Gromelski, M. Groth, O. Grover, M. Gruca, A. Gude, C. Guillemaut, R. Guirlet, J. Gunn, T. Gyergyek, L. Hagg, A. Hakola, J. Hall, C.J. Ham, M. Hamed, T. Happel, G. Harrer, J. Harrison, D. Harting, N.C. Hawkes, P. Heinrich, S. Henderson, P. Hennequin, R. Henriques, S. Heuraux, J. HidalgoSalaverri, J. Hillairet, J.C. Hillesheim, A. Hjalmarsson, A. Ho, J. Hobirk, E. Hodille, M. Hölzl, M. Hoppe, J. Horacek, N. Horsten, L. Horvath, M. Houry, K. Hromasova, J. Huang, Z. Huang, A. Huber, E. Huett, P. Huynh, Iantchenko, M. Imrisek, P. Innocente, C. IonitaSchrittwieser, H. Isliker, P. Ivanova, I. Ivanova Stanik, M. Jablczynska, S. Jachmich, A. S. Jacobsen,

P. Jacquet, A. Jansen van Vuuren, A. Jardin, H. Järleblad, A. Järvinen, F. Jaulmes, T. Jensen, I. Jepu, S. Jessica, E. Joffrin, T. Johnson, A. Juven, J. Kalis, A. Kappatou, J. Karhunen, R. Karimov, A. N. Karpushov, S. Kasilov, Y. Kazakov, PV. Kazantzidis, D. Keeling, W. Kernbichler, HT. Kim, D.B. King, V.G. Kiptily, A. Kirjasuo, K.K. Kirov, A. Kirschner, A. Kit, T. Kiviniemi, F. Kjær, E. Klinkby, A. Knieps, U.Knoche, M. Kochan, F. Köchl, G. Kocsis, J.T.W.koenders, L. Kogan, Y. Kolesnichenko, Y. Kominis, M. Komm, M. Kong, B. Kool, S. B. Korsholm, D. Kos, M. Koubiti, J. Kovacic, Y. Kovtun, E. KowalskaStrzeciwilk, K. Koziol, M. Kozulia, A. KrämerFlecken, A. Kreter, K. Krieger, U. Kruezi, O. Krutkin, O. Kudlacek, U. Kumar, H. Kumpulainen, M. H.Kushoro, R. Kwiatkowski, M. La Matin.

The members of the MAST-U Team are J. R. Harrison, A. Aboutaleb, S. Ahmed, M. Aljunid, S. Y. Allan, H. Anand, Y. Andrew, L. C. Appel, A. Ash, J. Ashton, O. Bachmann, M. Barnes, B. Barrett, D. Baver, D. Beckett, J. Bennett, J. Berkery, M. Bernert, W. Boeglin, C. Bowman, J. Bradley, D. Brida, P. K. Browning, D. Brunetti, P. Bryant, J. Bryant, J. Buchanan, N. Bulmer, A. Carruthers, M. Cecconello, Z. P. Chen, J. Clark, C. Cowley, M. Coy, N. Crocker, G. Cunningham, I. Cziegler, T. Da Assuncao, Y. Damizia, P. Davies, I. E. Day, G. L. Derks, S. Dixon, R. Doyle, M. Dreval, M. Dunne, B. P. Duval, T. Eagles, J. Edmond, H. El-Haroun, S. D. Elmore, Y. Enters, M. Faitsch, F. Federici, N. Fedorczak, F. Felici, A. R. Field, M. Fitzgerald, I. Fitzgerald, R. Fitzpatrick, L. Frassinetti, W. Fuller, D. Gahle, J. Galdon-Quiroga, L. Garzotti, S. Gee, T. Gheorghiu, S. Gibson, K. J. Gibson, C. Giroud, D. Greenhouse, V. H. Hall-Chen, C. J. Ham, R. Harrison, S. S. Henderson, C. Hickling, B. Hnat, L. Howlett, J. Hughes, R. Hussain, K. Imada, P. Jacquet, P. Jepson, B. Kandan, I. Katramados, Y. O. Kazakov, D. King, R. King, A. Kirk, M. Knolker, M. Kochan, L. Kogan, B. Kool, M. Kotschenreuther, M. Lees, A. W. Leonard, G. Liddiard, B. Lipschultz, Y. Q. Liu, B. A. Lomanowski, N. Lonigro, J. Lore, J. Lovell, S. Mahajan, F. Maiden, C. Man-Friel, F. Mansfield, S. Marsden, R. Martin, S. Mazzi, R. McAdams, G. McArdle, K. G. McClements, J. McClenaghan, D. McConville, K. McKay, C. McKnight, P. McKnight, A. McLean, B. F. McMillan, A. McShee, J. Measures, N. Mehay, C. A. Michael, F. Militello, D. Morbey, S. Mordijck D. Moulton, O. Myatra, A. O. Nelson, M. Nicassio, M. G. O'Mullane, H. J. C. Oliver, P. Ollus, T. Osborne, N. Osborne, E. Parr, B. Parry, B. S. Patel, D. Payne, C. Paz-Soldan, A. Phelps, L. Piron, C. Piron, G. Prechel, M. Price, B. Pritchard, R. Proudfoot, H. Reimerdes, T. Rhodes, P. Richardson, J. Riquezes, J. F. Rivero-Rodriguez, C. M. Roach, M. Robson, K. Ronald, E. Rose, P. Ryan, D. Ryan, S. Saarelma, S. Sabbagh, R. Sarwar, P. Saunders, O. Sauter, R. Scannell, T. Schuett, R. Seath, R. Sharma, P. Shi, B. Sieglin, M. Simmonds, J. Smith, A. Smith, V. A. Soukhanovskii, D. Speirs, G. Staebler, R. Stephen, P. Stevenson, J. Stobbs, M. Stott, C. Stroud, C. Tame, C. Theiler, N. Thomas-Davies, A. J. Thornton, M. Tobin, M. Vallar, R. G. L. Vann, L. Velarde, K. Verhaegh, E. Viezzer, C. Vincent, G. Voss, M. Warr, W. Wehner, S. Wiesen, T. A. Wijkamp, D. Wilkins, T. Williams, T. Wilson, H. R. Wilson, H. Wong, M. Wood, V. Zamkovska.

REFERENCES

[1] A. Fasoli et al., "Chapter 5: Physics of energetic ions," *Nucl. Fusion*, vol. 47, no. 6, p. S264, 2007.

[2] J. Galdon-Quiroga et al., "Velocity space resolved absolute measurement of fast ion losses induced by a tearing mode in the ASDEX upgrade tokamak," *Nucl. Fusion*, vol. 58, no. 3, Mar. 2018, Art. no. 036005.

[3] J. R. Harrison et al., "Overview of new MAST physics in anticipation of first results from MAST Upgrade," *Nucl. Fusion*, vol. 59, no. 11, 2019, Art. no. 112011.

[4] J. E. Menard et al., "Overview of NSTX Upgrade initial results and modelling highlights," *Nucl. Fusion*, vol. 57, no. 10, 2017, Art. no. 102006.

[5] C. A. Michael et al., "Dual view FIDA measurements on MAST," *Plasma Phys. Controlled Fusion*, vol. 55, no. 9, Sep. 2013, Art. no. 095007.

[6] G. Prechel et al., "Installation of a solid state neutral particle analyzer array on mega ampere spherical tokamak upgrade," *Rev. Sci. Instrum.*, vol. 93, no. 11, Nov. 2022, Art. no. 113517.

[7] M. Cecconello et al., "First observations of confined fast ions in MAST upgrade with an upgraded neutron camera," *Plasma Phys. Controlled Fusion*, vol. 65, no. 3, Mar. 2023, Art. no. 035013.

[8] A. Aboutaleb, "Proton detection in MAST-U using silicon and diamond surface barrier detectors," in *Proc. 63rd Annu. Meeting APS Division Plasma Phys.*, Pittsburg, PA, USA, 2021, pp. 1–17.

[9] J. F. Rivero-Rodriguez et al., "A rotary and reciprocating scintillator based fast-ion loss detector for the MAST-U tokamak," *Rev. Sci. Instrum.*, vol. 89, no. 10, Oct. 2018, Art. no. 10I112.

[10] S. J. Zweben, "Pitch angle resolved measurements of escaping charged fusion products in TFTR," *Nucl. Fusion*, vol. 29, no. 5, pp. 825–833, May 1989.

[11] S. Baeumel et al., "Scintillator probe for lost alpha measurements in JET," *Rev. Sci. Instrum.*, vol. 75, no. 10, pp. 3563–3565, Oct. 2004.

[12] J. F. Rivero-Rodriguez et al., "Upgrade and absolute calibration of the JET scintillator-based fast-ion loss detector," *Rev. Sci. Instrum.*, vol. 92, no. 4, Apr. 2021, Art. no. 043553.

[13] D. S. Darrow, "Scintillator based energetic ion loss diagnostic for the national spherical torus experiment," *Rev. Sci. Instrum.*, vol. 79, no. 2, Feb. 2008, Art. no. 023502.

[14] M. Garcia-Munoz et al., "Conceptual design of the ITER fast-ion loss detector," *Rev. Sci. Instrum.*, vol. 87, no. 11, Nov. 2016, Art. no. 11D829.

[15] M. Kocan et al., "The impact of the fast ion fluxes and thermal plasma loads on the design of the ITER fast ion loss detector," *J. Instrum.*, vol. 12, no. 12, Dec. 2017, Art. no. C12027.

[16] J. Ayllon-Guerola et al., "Dynamic and thermal simulations of a fast-ion loss detector for ITER," *Fusion Eng. Des.*, vol. 123, pp. 807–810, Nov. 2017.

[17] J. Galdon-Quiroga et al., "Velocity-space sensitivity and tomography of scintillator-based fast-ion loss detectors," *Plasma Phys. Controlled Fusion*, vol. 60, no. 10, Oct. 2018, Art. no. 105005.

[18] M. García-Muñoz et al., "Characterization of scintillator screens for suprathermal ion detection in fusion devices," *J. Instrum.*, vol. 6, no. 4, Apr. 2011, Art. no. P04002.

[19] D. Dunai, S. Zoletnik, J. Sárközi, and A. R. Field, "Avalanche photodiode based detector for beam emission spectroscopy," *Rev. Sci. Instrum.*, vol. 81, no. 10, Oct. 2010, Art. no. 103503.

[20] M. García-Muñoz, H.-U. Fahrbach, and H. Zohm, "Scintillator based detector for fast-ion losses induced by magnetohydrodynamic instabilities in the ASDEX upgrade tokamak," *Rev. Sci. Instrum.*, vol. 80, no. 5, May 2009, Art. no. 053503.

[21] J. Moritz, E. Faudot, S. Devaux, and S. Heuraux, "Plasma sheath properties in a magnetic field parallel to the wall," *Phys. Plasmas*, vol. 23, no. 6, Jun. 2016, Art. no. 062509.

[22] L. Velarde, "Velocity-space analysis of the first fast-ion losses measured in MAST-U using a high-speed camera in the FILD detector," in *Proc. 5th Eur. Conf. Plasma Diag.*, Crete, Greece, 2023, pp. 1–9.

[23] J. F. Rivero-Rodriguez, "First experimental measurements of the scintillator-based fast-ion loss detector in the MAST-U spherical tokamak," in *Proc. 5th Eur. Conf. Plasma Diag.*, Crete, Greece, 2023, pp. 6–69.

[24] J. F. Rivero-Rodriguez, "Overview of fast particle experiments in the first MAST-U experimental campaigns," in *Proc. 29th IAEA Fusion Energy Conf.*, London, U.K., 2023, p. 2104.